JOC The Journal of Organic Chemistry

Article

pubs.acs.org/joc

Isolation and Characterization of Persistent Radical Cation and Dication of 2,7-Bis(dianisylamino)pyrene

Ryohei Kurata, Kazuyoshi Tanaka, and Akihiro Ito*

Department of Molecular Engineering, Graduate School of Engineering, Kyoto University, Nishikyo-ku, Kyoto 615-8510, Japan

Supporting Information

ABSTRACT: Orbital interaction between 2,7-pyrenylene and two nitrogen redox-active centers effectively reduces the energy difference between HOMO and HOMO−1, both of which were distributed over the two nitrogen centers. In fact, one- and two-electron oxidation of 2,7-bis(dianisylamino)-pyrene **3** generated a persistent radical cation and a persistent dication, respectively, and we succeeded in the isolation and single crystal X-ray structural analyses of all three oxidation states. The radical cation was considered as a spin and charge delocalized mixed-valence compound with a semiquinoidal structure. The dication was in an open-shell singlet state with a small singlet−triplet energy gap. The molecular and electronic structures for all three oxidation states of **3** were studied in comparison with the data reported for each oxidation state of closely related bis(triarylamine)s, of which structures were determined by X-ray crystallography.

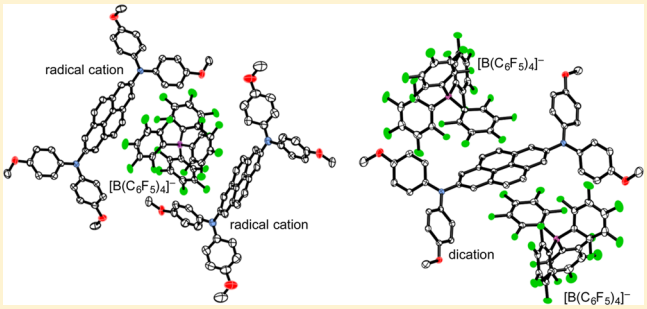

INTRODUCTION

Multistage organic redox systems have recently attracted renewed interest not only in view of practical applications as functional materials in molecular electronics, but also in view of a fundamental understanding of molecular and/or electronic structural changes upon each redox stage.[1] Among these redox systems, two-stage Wurster-type systems are known as well-characterized compounds from both experimental and theoretical viewpoints.[2] *Para*-phenylenediamines (**1**), the typical examples for the two-stage Wurster-type, are electron-rich compounds, and thus can be readily converted by one-electron oxidation into a stable semiquinone radical cation,[3] which can be further oxidized into a stable quinone dication (Figure 1).[4] As a counterpart of **1**, Kaim and co-workers established that electron-deficient *para*-phenylenediboranes (**2**) are considered as "mirror image" in terms of two-stage Wurster-type redox systems (Figure 1).[5] The validity of the B/N analogy has been confirmed also in 4,4′-biphenylene-bridged bis(triarylamine)s (**5**)[6] and bis(triarylborane)s (**6**).[7]

In these two-stage redox systems, the importance of π-conjugated bridges between two redox-active centers has also been frequently discussed, and therefore, several kinds of π-conjugated bridging units have been tested to clarify the influence on the electronic communication between the redox-active centers.[1b,2a] To extend the diversity of π-conjugated bridging units, a promising strategy is the use of polycyclic aromatic hydrocarbons (PAHs), which have characteristic electronic structures depending on the presence of so-called "edge state."[8] Pyrene is one of the simplest PAHs, and the pyrene derivatives are recognized as versatile chromophores[9] in their application to organic optoelectronics due to the fact that the selective functionalization of the pyrene core at bespoke positions other than the usual 1-, 3-, 6-, and 8-positions has become facilitated by the recent progress in synthetic organic chemistry.[10] In this context, we started investigating the possibility of pyrene as a novel π-conjugated bridging unit between nitrogen redox-active centers. In particular, 2,7-disubstituted pyrene derivatives are intriguing because of the existence of nodal plane in both the HOMO and LUMO passing through C2 and C7 carbon atoms of pyrene core (Figure 2a). In addition, the 2,7-pyrenylene moiety in 2,7-bis(dianisylamino)pyrene (**3**)[11] can be regarded as a planar-constrained biphenyl unit tethered by two —CH═CH— groups, thereby closely relating to the compounds **5a**. Prior to our present studies on **3**, 2,7-diruthenium metalated pyrene derivatives were reported to be in a mixed-valence state for their mono-oxidized forms,[12] in addition to reports on the mixed-valence states for bis(diarylamine) molecular systems bridged by a bis(terpyridine)ruthenium(II) moiety and metal-chelating 2,2′-bipyridines.[13] In addition, the electrochemical and spectroscopic propeties on pyrene derivatives with dianisylamino-substituents at 1-, 3-, 6-, and 8-positions were also demonstrated.[14]

Very recently, the isolation and characterization of radical anion and dianion of 2,7-bis(diarylborano)pyrene (**4**) have been reported by Marder and co-workers.[15] Their strategy is based on the theoretical prediction that an in-phase orbital interaction between the LUMO+1 of the pyrene core and the two vacant B 2p orbitals in **4** results in the delocalized

Received: October 20, 2015
Published: December 21, 2015

DOI: 10.1021/acs.joc.5b02425
J. Org. Chem. 2016, 81, 137−145

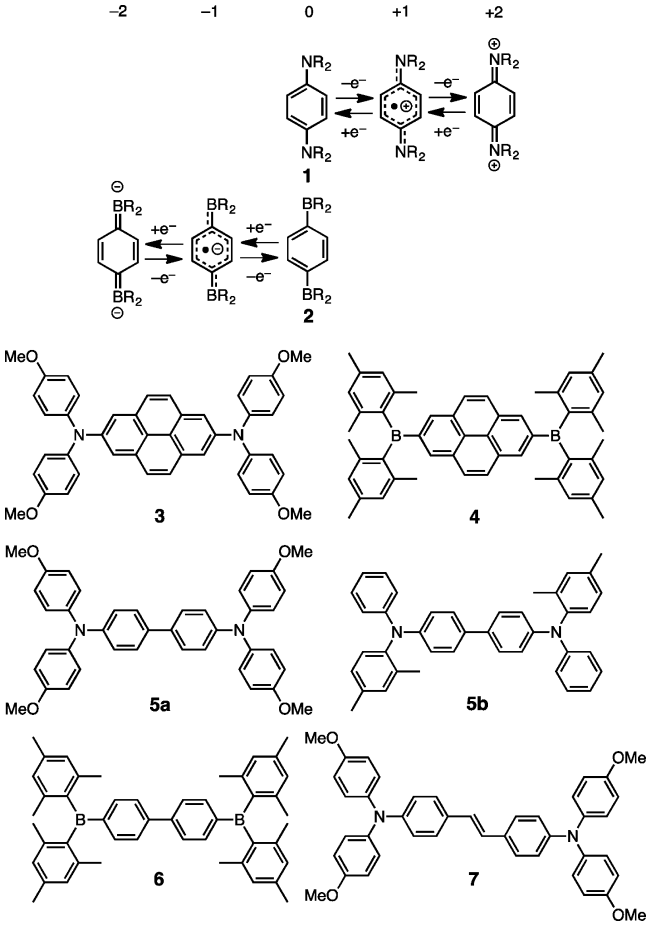

Figure 1. *Para*-phenylenediamine (**1**) and *Para*-phenylenediborane (**2**) as two-stage Wurster-type redox systems, and the closely related compounds **3**−**7**.

distribution of LUMO over the entire molecule of **4**, thus leading to a charge-delocalized semiquinoidal (**SQ**) radical anion and a closed-shell quinoidal (**Q**) dianion of **4**. As has been noticed independently by Marder and co-workers,[9h] we have also noticed that an out-of-phase orbital interaction between the HOMO−1 of the pyrene core and the two N 2p orbitals results in the delocalized distribution of HOMO over the entire molecule of **3** (Figure 2a). In addition, the HOMO−1 of **3** was found to be of nonbonding character with large MO coefficient at the two nitrogen redox-active centers, as a result of orbital mixing with LUMO+1 of the pyrene core in an in-phase fashion. As a consequence, the energy difference between the HOMO and HOMO−1 is effectively reduced for **3**, so that the preference of open-shell diradical character for the dication of **3** can be probably enhanced.

As shown in Figure 2b, similar in-phase and out-of-phase orbital interactions between the LUMO and HOMO of the biphenylene core and the two N 2p orbitals lead to the small energy difference between the HOMO and HOMO−1 in **5a**. The similarity in the frontier orbitals between **3** and **5a** entails, to some extent, a resemblance between 2,7-pyrenylene and 4,4′-biphenylene π-conjugated bridging units.

In this article, we present the preparation, X-ray structural elucidation, spectroscopic characterization and DFT-computational investigation of 2,7-bis(dianisylamino)pyrene **3**, its radical cation $\mathbf{3}^{\bullet+}$, and its dication $\mathbf{3}^{2+}$. The present bis(diarylamine) molecular system is still rare case where the

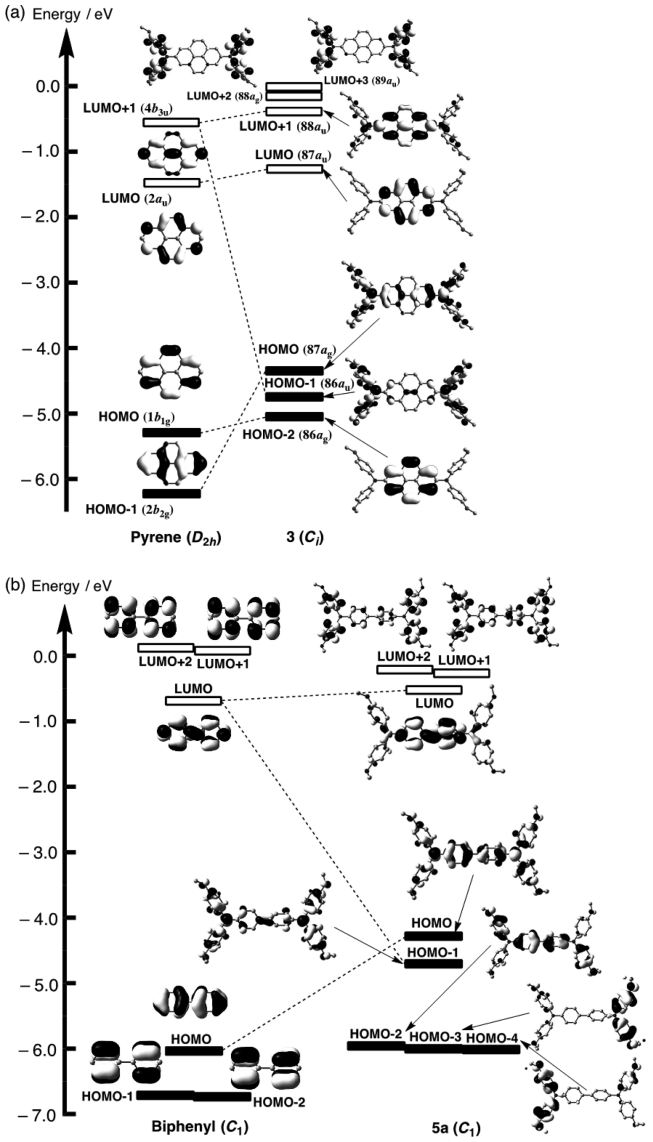

Figure 2. Schematic drawing of the frontier Kohn−Sham orbitals for (a) pyrene and **3** and (b) biphenyl and **5a** at the B3LYP/6-31G* level of theory. The HOMO and HOMO−1 of **3** originate from orbital interactions between the two N 2p orbitals and the HOMO−1 and LUMO+1 of the pyrene core, while the HOMO and HOMO−1 of **5a** from orbital interactions between the two N 2p orbitals and the HOMO and LUMO of the biphenyl core.

isolation and single crystal X-ray structural analyses of all three oxidation states have been successfully accomplished, such as the vinylene-bridged bis(triarylamine) **7**.[16]

■ RESULTS AND DISCUSSION

Compound **3** was obtained as yellow powder in 40% yield[17] from commercially available dianisylamine and 2,7-dibromopyrene[10a] by using the Palladium-catalyzed cross-coupling amination reaction.[18] Cyclic voltammetry (CV) and differential pulse voltammetry (DPV) of **3** in CH_2Cl_2 (0.1 M nBu$_4$N$^+$BF$_4^-$, 100 mV s^{-1}) at 298 K showed two successive one-electron-oxidation steps with clearly separated potentials [E_{ox}^1 = +0.136 V, E_{ox}^2 = +0.376 V, $\Delta E = E_{ox}^2 - E_{ox}^1$ = 240 mV], suggesting, to some extent, a resonance stabilization of the positive charge and the unpaired electron in $\mathbf{3}^{\bullet+}$ (Figure S2, Supporting Information). The ΔE value of **3** is comparable to those of

DOI: 10.1021/acs.joc.5b02425
J. Org. Chem. 2016, 81, 137−145

all-*N*-anisyl-substituted **5a** (ΔE = 300 mV; in CH_2Cl_2 at r.t. [0.1 M $nBu_4N^+BF_4^-$, 100 mV s^{-1}])[1b] and **4** (ΔE = 280 mV; in THF at r.t. [0.1 M $nBu_4N^+PF_6^-$, 250 mV s^{-1}]),[15] suggesting that 2,7-pyrenylene has similar strength as the electronic coupling unit to 4,4′-biphenylene. For comparison, electrochemical redox data of all compounds discussed here are listed in Table 1.

Table 1. Electrochemical Potentials (in V versus $Fc^{0/+}$) by Cyclic Voltammetry (Scan Rate: 0.1 V s^{-1}) of 3 and Related Compounds in CH_2Cl_2 (0.1 M n-Bu_4BF_4) at Room Temperature

compd	E_1	E_2	ΔE (= $E_2 - E_1$)
3	+0.136	+0.376	0.240
5a[a]	+0.250	+0.550	0.300
5b[b]	+0.250	+0.505	0.255
7[c]	+0.08	+0.22	0.14
pyrene[d]	+0.868	+1.848[e]	–
biphenyl[f]	+1.85[e]	–	–
stilbene[g]	+1.48	–	–

[a]Taken from ref 1b. [b]Taken from ref 6a. [c]Taken from ref 16a; measured in the presence of 0.1 M n-Bu_4PF_6 in CH_2Cl_2 and scan rate is 0.05 V s^{-1}. [d]Taken from ref 19; measured in the presence of 0.1 M n-Bu_4PF_6 in SO_2 at −52 °C and scan rate is 0.2 V s^{-1}. [e]Irreversible. [f]Taken from ref 20; measured in the presence of n-Bu_4PF_6 in CH_2Cl_2 at low temperature, high scan rate, and low substrate concentration (in V versus Ag/AgCl). [g]Taken from ref 21; measured in the presence of 0.1 M n-Bu_4ClO_4 in CH_3CN (in V versus Ag/AgCl).

To gain information about the electronic structure corresponding to $\mathbf{3}^{\bullet+}$ and $\mathbf{3}^{2+}$, the UV−vis−NIR absorption spectral change was monitored throughout the electrochemical oxidation of **3** in CH_2Cl_2. In the oxidation process from **3** to $\mathbf{3}^{\bullet+}$ (Figure 3a), three bands appeared at 0.65 (λ_{max} = 1900 nm), 1.77 (λ_{max} = 700 nm), and 2.76 eV (λ_{max} = 450 nm), and it should be noted that the lowest-energy band shape was considerably asymmetrical [the ratio of the bandwidth at half-height of the high-energy side and the low-energy side $\tilde{\nu}_{1/2}$(high)/$\tilde{\nu}_{1/2}$(low) = 2.36] (Figure S4, Supporting Information), which is characteristic of the charge-resonance (CR) intervalence (IV) band [Robin-Day's class III].[22] Hence, assuming the delocalized (class III) IV behavior, the value of the electronic coupling between two redox centers, V (=$\tilde{\nu}_{max}$/2), for **3** is estimated to be 2608 cm^{-1}, which is slightly smaller than that for all-*N*-anisyl-substituted **5a** (3410 cm^{-1}).[1b] To further evaluate the spin distribution, we measured the ESR spectrum of $\mathbf{3}^{\bullet+}$ generated by chemical oxidation with 0.5 equiv of Magic Blue[23] in CH_2Cl_2. The observed spectrum with five-line hyperfine structure was well simulated by the presence of two equivalent nitrogen nuclei ($|a_N|$ = 0.5 mT) and the contribution from unresolved hydrogen nuclei, which were incorporated in the line width of the spectral simulation (0.33 mT) (Figure S5, Supporting Information). In addition, the ESR spectral shape remained unchanged in the measured temperature range (193−293 K) (Figure S6, Supporting Information). The present ESR data are consistent with delocalization of the unpaired electron between two nitrogen redox-active centers, thus supporting assignment of $\mathbf{3}^{\bullet+}$ to class III system. The delocalized IV state of $\mathbf{3}^{\bullet+}$ can be supported also by time-dependent density functional (TD-DFT) calculations for the symmetrically charged structure of $\mathbf{3}^{\bullet+}$, which is preferentially optimized at the UB3LYP/6-31G* level.[24] The calculated delocalized spin density distribution is also consistent with the above-mentioned ESR observation ($|a_N|_{calc}$ = 0.42 mT) (Figure S7, Supporting Information), and furthermore, the lowest energy absorption band at 0.65 eV belongs to the electronic transition from β-HOMO [distributed on two N 2p orbitals in an in-phase fashion] to β-LUMO [distributed on two N 2p orbitals in an out-of-phase fashion], which is assignable to the CR IV state (Figure S7, Supporting Information). Therefore, it was confirmed that $\mathbf{3}^{\bullet+}$ is in a delocalized IV state like $\mathbf{4}^{\bullet-}$.

As shown in Figure 3b, further oxidation of $\mathbf{3}^{\bullet+}$ into dication $\mathbf{3}^{2+}$ was accompanied by rapid decrease of the CR IV band, and instead, by continuous increase of two bands at 1.38 eV (λ_{max} = 900 nm) and 1.62 eV (λ_{max} = 765 nm), which are assignable to a charge transfer excitation between two nitrogen redox-active centers (1.22 eV (f = 0.23)) and a charge transfer excitation within a nitrogen redox-center (1.70 eV (f = 0.46)), respectively, judging from the TD-DFT calculations for the optimized geometries of $\mathbf{3}^{2+}$ with an broken-symmetry (BS) open-shell singlet (OSS) state (Figure S8, Supporting Information). Note that, however, the computed transition

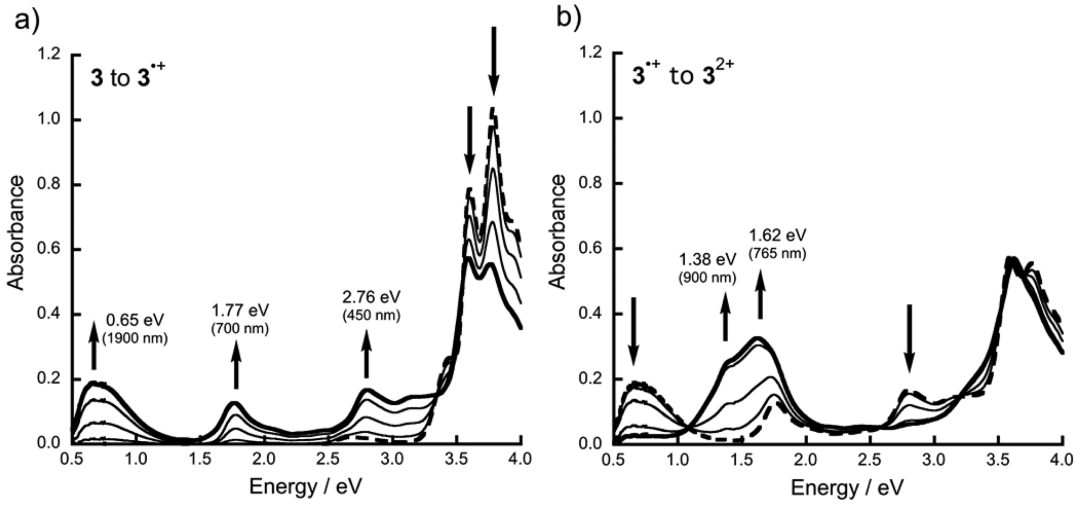

Figure 3. UV−vis−NIR absorption spectra of the stepwise electrochemical oxidation of **3** in CH_2Cl_2 with 0.1 M nBu_4NBF_4 at 298 K: (a) **3** to $\mathbf{3}^{\bullet+}$; (b) $\mathbf{3}^{\bullet+}$ to $\mathbf{3}^{2+}$.

DOI: 10.1021/acs.joc.5b02425
J. Org. Chem. 2016, 81, 137−145

energies (1.11 eV (f = 1.15) and 1.82 eV (f = 0.45)) for the closed-shell singlet (CS) geometry for 3^{2+} have some similarity to the observed lowest-energy bands. In this situation, we cannot rule out the possibility that the electronic structure of 3^{2+} is not well documented as a pure single configuration. In fact, the single point CAS(2,2)/6-31G* calculation at the DFT-optimized OSS geometry for 3^{2+} showed that the fractional occupation numbers of the HOMO and LUMO were estimated to be 1.11 and 0.89, respectively, thus suggesting that the CS configuration can be mixed to some extent.

The chemical oxidation of **3** was conducted by using $Ag[B(C_6F_5)_4]$[25] as an oxidant in CH_2Cl_2, and successfully, the corresponding salts containing the weakly coordinating anion,[26] $3^{\bullet+}\cdot[B(C_6F_5)_4]^-$ and $3^{2+}\cdot 2[B(C_6F_5)_4]^-$, were separately isolated as stable black and deep-blue solids, respectively, by tuning a quantity of the oxidant. The isolated salts completely reproduce the same absorption spectra in CH_2Cl_2 (Figure S9, Supporting Information) as those for the electrochemically generated $3^{\bullet+}$ and 3^{2+} (Figure 3). Single crystals suitable for X-ray analyses were obtained by slow diffusion of *n*-hexane into the corresponding CH_2Cl_2 solution at −20 °C.[27] In addition, a slow evaporation from CH_2Cl_2/MeOH solution gave single crystals of **3**.[21] The isolated salts were highly stable at ambient conditions, and showed no spectral change for at least several months in air at −20 °C. The structures of neutral **3**, radical cation $3^{\bullet+}$, and dication 3^{2+} are shown in Figure 4, and their geometrical parameters are listed in Table 2. The neutral molecule **3** possesses a crystallographic inversion center in the crystal. As shown in Figure 4b, the crystal contains two crystallographically independent radical cations $3^{\bullet+}$(I) and $3^{\bullet+}$(II), both of which are located on crystallographic inversion centers, and separated by the $[B(C_6F_5)_4]$ anion, while the dication 3^{2+} does not lie on any symmetric centers and are fully separated from adjacent dication molecules in a sandwiched fashion by the two $[B(C_6F_5)_4]$ anions (Figure 4c). Turning now to the structural change of the 2,7-pyrene bridging unit of **3** during the two-step oxidation, there exist clear difference from that of "charge-reverse" analogue **4** during two-step reduction. As shown in Figure 4d, concerning the dihedral angle between the NC_3 and pyrene planes, the distinct reduction are not seen on the diaminopyrene **3**, $3^{\bullet+}$ and 3^{2+} (31−43°), whereas the dihedral angle between the BC_3 and pyrene planes clearly decreases with increasing reduction number on the diboranopyrene **4** (31.7°), $4^{\bullet-}$ (14.2°), and 4^{2-} (9.8°) as "charge-reverse" analogues, thus closely relating to the structural change to the **Q** structure through the **SQ** one.[15] This trend was also verified by the DFT optimized geometries of **3** (34.8°), $3^{\bullet+}$ (31.3°), and 3^{2+} (32.7° for the CS state, 42.9° for the BS-OSS state, and 45.8° for the triplet state). As is apparent from Table 2, the straightforward shortening and elongation of each bond lengths were not so evident in $3^{\bullet+}$ and 3^{2+}, in contrast to the significant change in bond lengths of **4**, $4^{\bullet-}$, and 4^{2-}. For instance, the observed bond-length alternation (BLA) of the biphenyl moiety in the pyrene core (0.022−0.030 Å and 0.026 Å for $3^{\bullet+}$ and 3^{2+}, respectively) remains elusive,[28] whereas the corresponding BLA clearly increases with increasing reduction number of **4** (0.033 and 0.058 Å for $4^{\bullet-}$ and 4^{2-}, respectively).[15] Nevertheless, judging both from the DFT-computed BLA (0.025 Å) of $3^{\bullet+}$ and from the observed spin and charge delocalization in $3^{\bullet+}$, it can be safely said that the radical cation $3^{\bullet+}$ adopts a **SQ** structure, also in conjunction with the recently reported **SQ** structure for a 2,7-bisnitroxide-substituted pyrene derivative (BLA = 0.020 Å).[29] On the other hand, the X-ray structure of 3^{2+} resembles the optimized BS-OSS structure rather than the optimized CS structure on the basis of (U)B3LYP/6-31G* level. As a consequence, the low BLA value can be considered as an indication for diradical character of 3^{2+}. However, it should be noted that, as for 3^{2+}, the experimental $N-C_{pyrene}$ bond length is actually closer to that calculated for the CS state than the OSS one; the experimentally determined BLA (0.026 Å) takes an intermediate value between 0.035 and 0.014 Å which were estimated for the CS and OSS, respectively; the dihedral angle between the NC_3 and pyrene planes (33−34°) is also closer to that optimized for the CS state than OSS one. Hence, again, we cannot discard the possibility that the electronic structure of 3^{2+} is virtually multiconfigurational one; alternatively, the possibility that the present experimental observation is explainable by an equilibrium mixture of the CS and OSS species. Additionally, it should be noted that electron-donating *N*-anisyl groups are substituted for **3** to stabilize the oxidized species by mesomeric effect, while *B*-mesityl groups substituted for **4** to protect the boron center by kinetic stabilization due to sterically congestion. Hence, the twisted mesityl group hinders the effective conjugation with the vacant B 2p orbital, in return, leading to strengthen the conjugation between the vacant B 2p orbital and the bridging pyrene π-face for the reduced species of **4**. On the other hand, the oxidized species of **3** are expected to

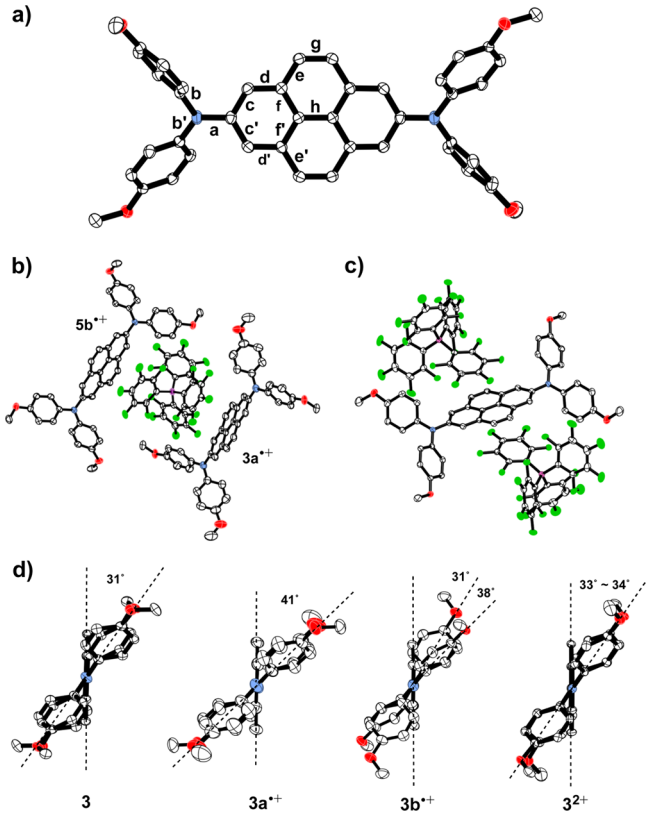

Figure 4. ORTEP drawings of (a) **3**, (b) $3^{\bullet+}\cdot[B(C_6F_5)_4]^-$ and (c) $3^{2+}\cdot 2[B(C_6F_5)_4]^-$, as determined from X-ray structural analyses at 93 K, and (d) side views of the dihedral angle between the NC_3 and pyrene planes. Crystallization solvent molecules (*n*-hexane for $3^{\bullet+}\cdot[B(C_6F_5)_4]^-$ and $3^{2+}\cdot 2[B(C_6F_5)_4]^-$) and hydrogen atoms are omitted for clarity; boron, nitrogen, oxygen, and fluorine atoms are colored in purple, blue, red, and green, respectively; the thermal ellipsoids are shown at the 50% probability level.

DOI: 10.1021/acs.joc.5b02425
J. Org. Chem. 2016, 81, 137−145

Table 2. Comparison of Bond Lengths (Å) Determined by X-ray Structural Analyses at 93 K and the DFT Optimized Bond Lengths for 3, $3^{\bullet+}$ and 3^{2+}

bond	3	$3^{\bullet+}$(I)	$3^{\bullet+}$(II)	3^{2+}
a	1.4083(19)	1.410(7)	1.403(6)	1.403(2) [1.399(2)][a]
b, b′	1.4274(17), 1.4227(19)	1.428(7), 1.418(7)	1.431(6), 1.411(6)	1.396(2), 1.419(2) [1.412(2), 1.416(2)][a]
c, c′	1.3957(19), 1.3959(19)	1.395(7), 1.398(7)	1.398(6), 1.399(6)	1.406(2), 1.407(3) [1.404(2), 1.409(3)][a]
d, d′	1.391(2), 1.392(2)	1.389(7), 1.389(7)	1.382(7), 1.378(6)	1.392(2), 1.385(2) [1.386(2), 1.383(2)][a]
e, e′	1.4384(19), 1.4394(18)	1.413(7), 1.434(7)	1.439(7), 1.448(7)	1.446(2), 1.443(3) [1.440(2), 1.441(3)][a]
f, f′	1.4241(17), 1.4189(18)	1.436(7), 1.427(7)	1.433(6), 1.431(6)	1.429(3), 1.425(2) [1.433(3), 1.428(2)][a]
g	1.356(2)	1.345(8)	1.336(7)	1.349(2) [1.349(2)][a]
h	1.416(2)	1.404(7)	1.405(6)	1.410(2)
BLA[b]	0.012(1)	0.022(5)	0.030(4)	0.026(1)

bond	3_{calc}[c]	$3^{\bullet+}{}_{calc}$[d]	$3^{2+}{}_{calc}$ (CS)[c,e]	$3^{2+}{}_{calc}$ (OS)[d,e]	$3^{2+}{}_{calc}$ (T)[d,e]
a	1.426	1.401	1.396	1.424	1.430
c, c′	1.404	1.411	1.416	1.404	1.402
d, d′	1.400	1.393	1.389	1.399	1.400
e, e′	1.439	1.442	1.443	1.440	1.439
f, f′	1.427	1.433	1.438	1.431	1.429
g	1.362	1.359	1.358	1.360	1.361
h	1.422	1.412	1.405	1.420	1.423
BLA[b]	0.011	0.025	0.035	0.014	0.011

[a]Additional bond lengths due to the asymmetric structure of 3^{2+} in the crystalline state. [b]Bond-length alternation (BLA in Å) of the biphenyl moiety in the pyrene core, that is defined by the difference between the average of all **c**, **c**′, **f** and **f**′ bond lengths and the average all **d**, **d**′ and h bond lengths. [c]Calculated at the B3LYP/6-31G* level. [d]Calculated at the UB3LYP/6-31G* level. [e]CS = closed-shell singlet, OS = Open-shell broken-symmetry singlet, *T* = triplet.

prefer the delocalized structures including peripheral anisyl groups, thus leading to an open-shell diradical character for 3^{2+}.

Here it is worth mentioning more explicit comparison of the geometrical features in the present 2,7-pyrenylene-bridged systems, **3**, and other crystallographically clarified bis(diarylamine) systems, **5** and **7**. Schematic drawings of structural characteristics for three oxidation states of compounds **3**, **5**, and **7** are depicted in Figure 5. First of all, it should be noted that, out of these three bis(triarylamine) derivatives, compound **3** undergoes the smallest structural changes from neutral to dication states. In particular, the N–$C_{pyrenyl}$ bond length remains sparing at each oxidation state. For $3^{\bullet+}$, both of two crystallographically independent radical cation molecules, $3^{\bullet+}$(I) and $3^{\bullet+}$(II), adopt centrosymmetric structures, strongly suggesting the delocalized class III species of $3^{\bullet+}$, at least in the solid state. However, differences in geometrical parameters between $3^{\bullet+}$(I) and $3^{\bullet+}$(II) are slightly large, implying that solid-state packing arrangements sensitively affect the molecular structures. In the case of 3^{2+}, BLAs of phenyl rings in peripheral anisyl groups clearly displays **SQ** distortion, in line with the shortening of O–C_{phenyl} bond lengths in their anisyl groups. As described before, preference of open-shell diradical character for 3^{2+} is likely to be closely related to this mesomeric effect by electron-donating *N*-anisyl groups. In contrast, the geometrical change from neutral to radical cation in the 4,4′-biphenylene-bridged bis(triarylamine) **5b** is conspicuous (Figure 5b).[6a] The torsion angle between two phenylene rings in 4,4′-biphenylene moiety decreases from 37° in **5b** to 4° in $\mathbf{5b}^{\bullet+}$, in parallel with induction of the **SQ** bond

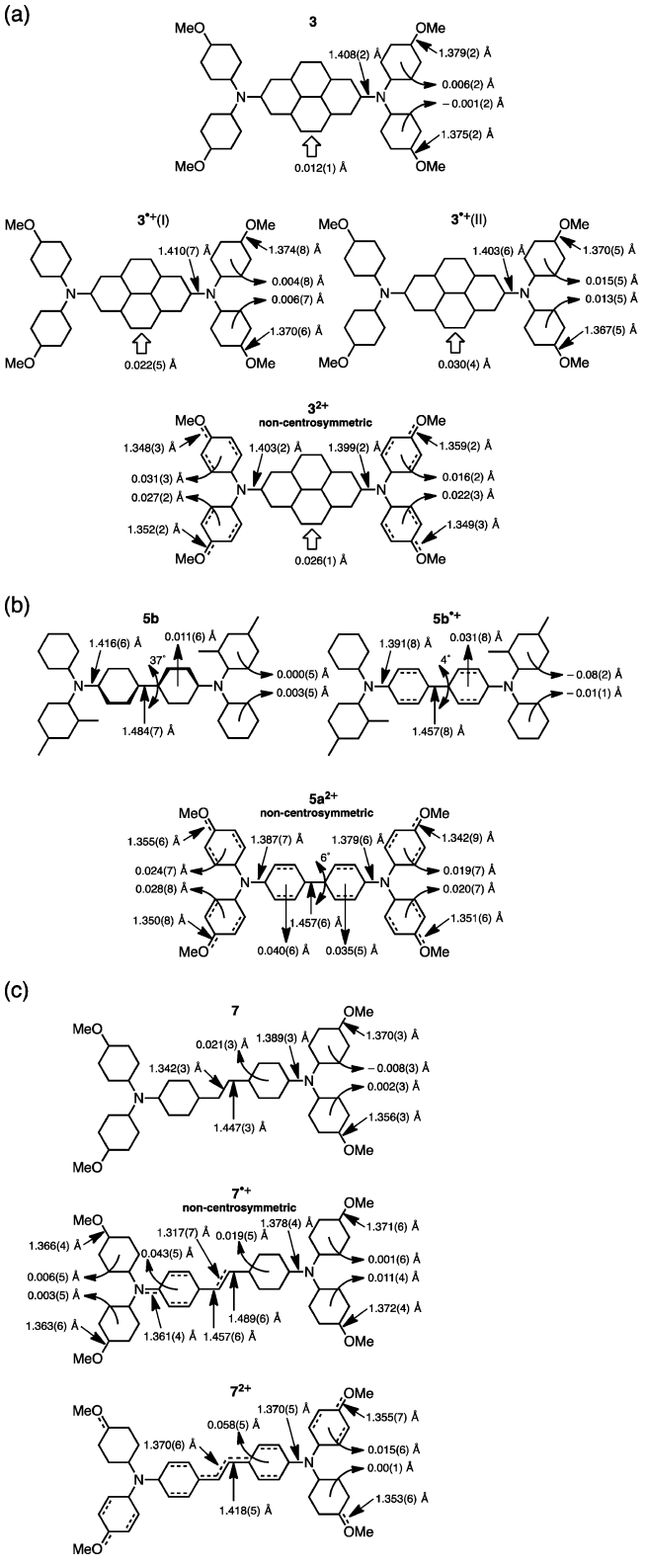

Figure 5. Schematic drawings of structural characteristics for three oxidation states of compounds **3**, **5** and **7** on the basis of X-ray structural analyses. Data for **5b** and $\mathbf{5b}^{\bullet+}$, $\mathbf{5a}^{2+}$ and the neutral to dication of **7** are taken from refs 6c, 6a, and 16, respectively. The value shown at the tip of an arrow from each phenyl ring designates the bond-length alternation (BLA in Å) for the phenyl ring, and the value shown at the bottom of a bold arrow designates the BLA of the biphenyl moiety in each pyrene core.

DOI: 10.1021/acs.joc.5b02425
J. Org. Chem. 2016, 81, 137–145

alternation of the 4,4′-biphenylene moiety upon one-electron oxidation of **5b** (BLA = 0.031 Å), and again, the centrosymmetric structures suggests the delocalized class III species of $\mathbf{5b}^{\bullet+}$, at least in the solid state. On the other hand, the **Q** deformation is not so strengthened for the 4,4′-biphenylene moiety in dication $\mathbf{5a}^{2+}$ with diradical character, whereas the **SQ** bond alternation of phenyl rings in the peripheral anisyl groups is clearly confirmed.[6c] However, the N−$C_{biphenyl}$ bond lengths for $\mathbf{5a}^{2+}$ [1.379(6) and 1.387(7) Å] were obviously short as compared with the N−$C_{pyrenyl}$ bond lengths for $\mathbf{3}^{2+}$ [1.399(2) and 1.403(2) Å], thus suggesting the weakeness of diradical character of $\mathbf{5a}^{2+}$. In the vinylene-bridged bis(triarylamine) **7**, radical cation $\mathbf{7}^{\bullet+}$ adopts an asymmetric structure in the solid state, although the counteranion is positioned right above the middle of the cation (Figure 5c).[16a] A **SQ** bond alternation is observed only for one of two triarylamine redox centers, suggesting an asymmetric charge localization as is seen in class II mixed-valence system. On the other hand, the diamagnetic dication $\mathbf{7}^{2+}$ takes a centrosymmetric structure in the solid state, and the bond alternation in the vinylene-bridge for dication $\mathbf{7}^{2+}$ is considerably reduced, although a **Q** deformation (BLA = 0.058 Å) in the phenylene moieties directly connected to the vinylene-bridge is observed in parallel with a **SQ** deformation in the peripheral anisyl groups.[16b]

To support the diradical character of $\mathbf{3}^{2+}$, the magnetic properties of $\mathbf{3}^{2+}$ were examined by the ESR spectroscopy and magnetic susceptibility measurements by using the SQUID magnetometer. The powder sample of $\mathbf{3}^{2+}$ also displayed a ESR signal with no definite fine-structure and moreover the intensity integral I for the observed signal increases with increasing temperature (T), and the singlet−triplet energy gap (ΔE_{S-T}) was estimated to be −2.92 kcal mol^{-1} from fitting with the singlet−triplet model equation[24] for the IT versus T plot (Figure 6). Corroboration for a diradical character of $\mathbf{3}^{2+}$ with a thermally accessible excited triplet state was provided by the SQUID measurements for the powder sample in the temperature range between 2 and 350 K at 0.1 T (Figure 7). An increase of the $\chi_M T$ value above 200 K was observed, and again,

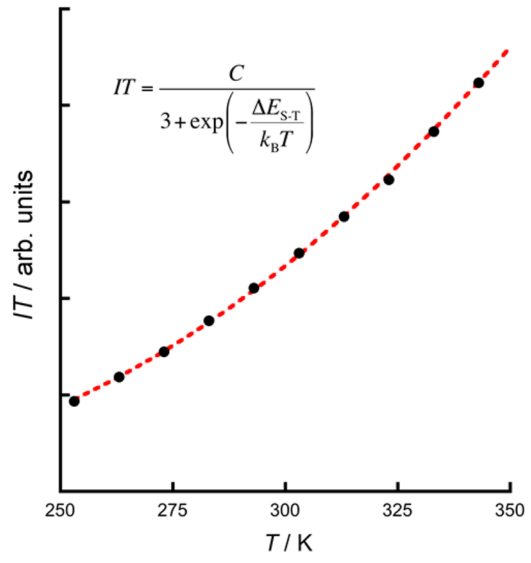

Figure 6. IT versus T plot [I is the observed ESR intensity integral for $\mathbf{3}^{2+}\cdot 2[B(C_6F_5)_4]^-$], and the best theoretical fit [the equation in the inset] to the data (broken red line; see text).

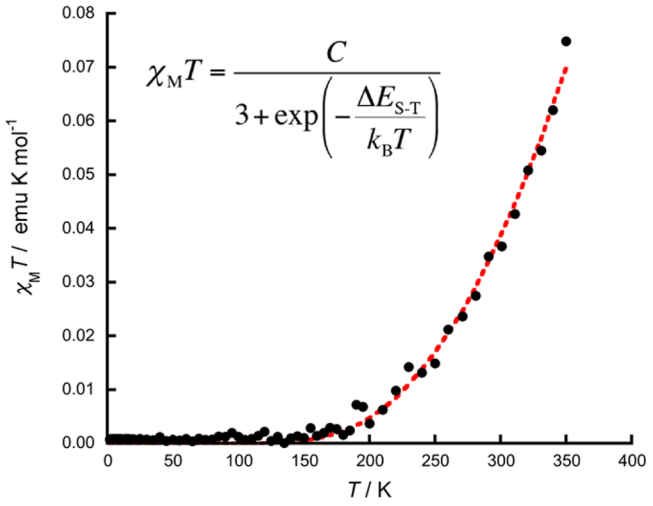

Figure 7. Plot of $\chi_M T$ versus T for $\mathbf{3}^{2+}\cdot 2[B(C_6F_5)_4]^-$ at 0.1 T. The broken line represents the best theoretical fit [the equation in the inset] to the data.

the energy gap ΔE_{S-T} for $\mathbf{3}^{2+}$ was obtained to be −2.58 kcal mol^{-1} from the best fitting with the singlet−triplet model equation,[30] clearly indicating that the energy gap ΔE_{S-T} determined by SQUID measurements is in good agreement with that determined by the ESR measurements. In addition, the S−T gap by the DFT-based BS approarch[31] was evaluated to be −1.43 kcal mol^{-1} at the UB3LYP/6-31G* level, which is in good accordance with the experimental values. As a consequence, the estimated S−T gap for the present dication $\mathbf{3}^{2+}$ was comparable to that of the dication of 4,4′-biphenylene-bridged bis(trianisylamine) $\mathbf{5a}^{2+}$ (−2.8 kcal mol^{-1}). Taking account of the clear difference between the N−$C_{biphenyl}$ bond lengths in $\mathbf{5a}^{2+}$ and the N−$C_{pyrenyl}$ bond lengths in $\mathbf{3}^{2+}$, this similarity would be quite interesting.

CONCLUSION

We have reported the isolation, crystal structures and electronic structures for all three oxidation states of 2,7-pyrenylene-bridged bis(trianisylamine) **3**. The present work elucidated the similarity and difference between the present compound **3** and other crystallographically clarified bis(triarylamine) analogues **5**[6] and **7**:[16] (1) the orbital interaction between the HOMO−1 and LUMO+1 of pyrene core and two pairs of N 2p orbitals in **3** resulted in the small energy gap between the HOMO and HOMO−1, both of which are distributed over two nitrogen centers, and the similar orbital interaction between the HOMO and LUMO of biphenyl core and two pairs of N 2p was also expected for 4,4′-biphenylene-bridged bis(triarylamine) **5**; (2) the spin and charge in $\mathbf{3}^{\bullet+}$ and $\mathbf{4}^{\bullet-}$ are delocalized over the entire molecular backbone despite of the difference in their **SQ** structural change; (3) the dication $\mathbf{3}^{2+}$ has an open-shell singlet diradical character with a thermally readily accessible triplet state at room temperature, probably originating from the relatively small energy gap between HOMO and HOMO−1 in **3**. Interestingly, the dication $\mathbf{5a}^{2+}$ is also regarded as a similar open-shell singlet diradical species,[6c] despite of the clear difference between the N−$C_{biphenyl}$ bond lengths in $\mathbf{5a}^{2+}$ and the N−$C_{pyrenyl}$ bond lengths in $\mathbf{3}^{2+}$. The preference of the diradical character for both $\mathbf{3}^{2+}$ and $\mathbf{5a}^{2+}$ is rather likely to be closely related to the **SQ** deformation in the peripheral anisyl groups. In contrast, for dication $\mathbf{7}^{2+}$, the bond alternation in the

DOI: 10.1021/acs.joc.5b02425
J. Org. Chem. 2016, 81, 137−145

vinylene-bridge is considerably reduced, and it should be noted that 7^{2+} was found to be in the closed-shell singlet state, although a **SQ** deformation in the peripheral anisyl groups is clearly observed.[16b]

EXPERIMENTAL SECTION

General Information. All the purchased reagents were of standard quality, and used without further purification. All the purchased solvents were purified, dried, and degassed by standard procedures. Column chromatography was performed with silica gel (neutral (pH 7.0 ± 0.5) spherical grain 40−100 μm in diameter). ^{1}H and ^{13}C NMR spectra were measured by a commercial 400 MHz FT-NMR spectrometer. Chemical shifts of NMR spectra are determined relative to internal tetramethylsilane (TMS) standard (δ), and are given in parts per million (ppm). UV−vis−NIR absorption spectra were obtained with a commercial optical absorption spectrometer. Fluorescence spectra were recorded on an commercial absolute photoluminescence quantum yield measurement system.

Electrochemical Measurements. The redox properties were evaluated by cyclic voltammetry and differential pulse voltammetry in CH_2Cl_2 solution at 298 K with 0.1 M tetra-*n*-butylammonium tetrafluoroborate ($TBABF_4$) as supporting electrolyte (scan rate 100 mV s^{-1}) using a commercial electrochemical analyzer. A three-electrode assembly was used, which was equipped with a platinum disk (2 mm^2) and a platinum wire as the working and counter electrodes, respectively, and Ag/0.01 M $AgNO_3$ (acetonitrile) was used as the reference electrode. The redox potential were referenced against a ferrocene/ferrocenium ($Fc^{0/+}$) redox potential measured in the same electrolytic solution.

Spectroelectrochemical Measurements. Spectroelectrochemical measurements were carried out with a custom-made optically transparent thin-layer electrochemical (OTTLE) cell (light pass length = 1 mm) equipped with a platinum mesh and a platinum coil as the working and counter electrodes, respectively, and Ag/0.01 M $AgNO_3$ (acetonitrile) was used as the reference electrode. The potential was applied with an commercial electrochemical analyzer.

ESR Measurements. ESR spectra were recorded on a commercial X-band ESR spectrometer, in which temperature was controlled by a commercial variable-temperature unit in the range of 193−293 K.

Magnetic Susceptibility Measurements. The magnetic susceptibility of polycrystalline samples of $\mathbf{3}^{\bullet+}$ and $\mathbf{3}^{2+}$ were measured by a commercial SQUID magnetometer in the temperature range 2K and 350 K at a constant magnetic field of 0.1 T. The raw data were corrected for both the magnetization of the sample holder alone and the diamagnetic contribution of the sample itself. The estimation of the diamagnetic contribution was done by using the Pacault method.[32] The temperature dependence of the molar magnetic susceptibility (χ_M) for $\mathbf{3}^{\bullet+}$ is shown in Figure S11 in the SI. At high-temperature region, the $\chi_M T$ value for $\mathbf{3}^{\bullet+}$ is in good agreement with the theoretical value of 0.375 emu K mol^{-1} expected for isolated 1/2 spins. On the other hand, the $\chi_M T$ value gradually decreased with decreasing temperature, indicating the intermolecular antiferromagnetic interactions. According to the spin polarization rule, the intramolecular spin−spin interactions in $\mathbf{3}^{\bullet+}$ are expected to be antiferromagnetic.

DFT Calculations. Quantum chemical calculations were performed with using a hybrid Hartree−Fock/density functional theory (HF/DFT) method (B3LYP).[33] Full geometrical optimization for **3**, $\mathbf{3}^{\bullet+}$, and $\mathbf{3}^{2+}$ was carried out and furthermore, their local minimum structures were confirmed by performing subsequent frequency analyses. Excitation energies for **3**, $\mathbf{3}^{\bullet+}$, and $\mathbf{3}^{2+}$ were examined on the basis of the time-dependent density functional method (TD-DFT)[34] with the same functional. All the computations employed the 6-31G* basis set.[35] All these computational approaches are implemented in Gaussian 09 package of ab initio MO calculation.[36]

Synthesis of 3. A mixture of 2,7-dibromopyrene (181 mg, 0.50 mmol), 4,4′-Dimethoxydiphenylamine (316 mg, 1.38 mmol), $Pd(dba)_2$ (8.0 mg, 0.014 mmol), $P(t\mathrm{Bu})_3HBF_4$ (15 mg, 0.052 mmol), and NaO*t*Bu (144 mg, 1.50 mmol) in toluene (10 mL) was stirred under an argon atmosphere at 110 °C for 19 h. After evacuation of the solvent, the residue was dissolved in dichloromethane and washed with brine. The organic layer was separated and dried over Na_2SO_4. After evaporation of the solvent, the crude product was chromatographed on silica gel (hexane/dichloromethane = 4/5 as eluent), and recrystallized from chloroform/ethanol to give **3** (132 mg, 40%) as a yellow solid: mp >300 °C; ^{1}H NMR (400 MHz, $CDCl_3$) δ = 3.82 (s, 12H), 6.86 (d, J = 8.8 Hz, 8H), 7.13 (d, J = 8.8 Hz, 8H), 7.66 (s, 4H), 7.69 (s, 4H); ^{13}C NMR (100 MHz, $CDCl_3$) δ = 55.5, 114.7, 118.2, 120.3, 126.1, 127.0, 131.2, 141.5, 146.0, 155.5. Anal. Calcd for $C_{44}H_{36}N_2O_4$: C, 80.47; H, 5.52; N, 4.27. Found: C, 80.27; H, 5.58; N, 4.03.

Synthesis of $\mathbf{3}^{\bullet+}\cdot[B(C_6F_5)_4]^-$. Compound **3** (13.1 mg, 0.02 mmol) was dissolved in dichloromethane (10 mL), and $Ag[B(C_6F_5)_4]$ (19.5 mg, 0.022 mmol) was added into the solution of **3** until the intensity of the lowest energy charge-resonance band (Figure 3a in the text) reached at its maximum by monitoring the absorption spectrum of the solution. The resulting solution was filtered through a syringe filter, and the filtrate was then concentrated (to about 2 mL) under vacuum. Three mL of *n*-hexane was layered directly over the filtrate, and it was stored at around −20 °C for 1 day to afford black crystals. The elemental analysis of this compound did not fit within 0.4% of the calculated values for the proposed formula probably due to the loss and/or the nonstoichiometric inclusion of *n*-hexane molucules.

Synthesis of $\mathbf{3}^{2+}\cdot 2[B(C_6F_5)_4]^-$. Compound **3** (13.1 mg, 0.02 mmol) was dissolved in dichloromethane (10 mL), and $Ag[B(C_6F_5)_4]$ (35.0 mg, 0.04 mmol) was added into the solution of **3** until the lowest energy charge-resonance band (Figure 3b in the text) completely dissapeared by monitoring the absorption spectrum of the solution. The resulting solution was filtered through a syringe filter, and the filtrate was then concentrated (to about 2 mL) under a vacuum. Five mL of *n*-hexane was layered directly over the filtrate, and it was stored at around −20 °C for 1 day to afford deep-blue crystalline powder. The elemental analysis of this compound did not fit within 0.4% of the calculated values for the proposed formula probably due to the loss and/or the nonstoichiometric inclusion of *n*-hexane molucules.

X-ray Analysis. Data collections were carried out on a commercial X-ray diffractometer using multilayer mirror monochromated Cu Kα radiation (λ = 1.54187 Å) from a rotating anode operating at 40 kV and 30 mA, and equipped with a hybrid pixel array detector. The samples were placed directly into a nitrogen stream at −180 ± 1 °C. The data were corrected for Lorentz and polarization effects. The structure was solved with the CrystalStructure crystallographic software package[37] using direct methods, and expanded by using Fourier techniques, and refined by full-matrix least-squares minimization by using SHELXL-97.[38] The non-hydrogen atoms were refined anisotropically. Hydrogen atoms were included in the refinement but restrained to ride on the atom to which they are bonded. The crystals of $\mathbf{3}^{\bullet+}\cdot[B(C_6F_5)_4]^-$ and $\mathbf{3}^{2+}\cdot 2[B(C_6F_5)_4]^-$ contain *n*-hexane molecules, which were used as one of the mixed solvents. The *n*-hexane molecules in the crystal of $\mathbf{3}^{\bullet+}\cdot[B(C_6F_5)_4]^-$ were partly disordered and treated properly.

ASSOCIATED CONTENT

Supporting Information

The Supporting Information is available free of charge on the ACS Publications website at DOI: 10.1021/acs.joc.5b02425.

X-ray crystallographic data of compound **3**. (CIF)

X-ray crystallographic data of compound $\mathbf{3}^{\bullet+}\cdot[B(C_6F_5)_4]^-$. (CIF)

X-ray crystallographic data of compound $\mathbf{3}^{2+}\cdot 2[B(C_6F_5)_4]^-$. (CIF)

^{1}H and ^{13}C NMR spectra of **3**, and additional electrochemical, optical spectroscopic, ESR spectroscopic, magnetic susceptibility measurements, and DFT computed data. (PDF)

DOI: 10.1021/acs.joc.5b02425
J. Org. Chem. 2016, 81, 137−145

AUTHOR INFORMATION

Corresponding Author

*E-mail: aito@scl.kyoto-u.ac.jp.

Notes

The authors declare no competing financial interest.

ACKNOWLEDGMENTS

The present work was partly supported by Grant-in-Aid for Scientific Research on Innovative Areas "New Polymeric Materials Based on Element-Blocks (No. 2401)" (Nos. 24102014 and 15H00734) from the Ministry of Education, Culture, Sports, Science, and Technology of Japan (MEXT). Numerical calculations were partly performed at the Supercomputer System of Kyoto University (Japan) and the Research Center for Computational Science in Okazaki (Japan). The authors would like to thank Dr. Takashi Matsumoto, Rigaku Corporation, for the X-ray analyses.

REFERENCES

(1) (a) Deuchert, K.; Hünig, S. *Angew. Chem., Int. Ed. Engl.* **1978**, *17*, 875−886. (b) Heckman, A.; Lambert, C. *Angew. Chem., Int. Ed.* **2012**, *51*, 326−392. (c) Wenger, O. S. *Chem. Soc. Rev.* **2012**, *41*, 3772−3779. (d) Parthey, M.; Kaupp, M. *Chem. Soc. Rev.* **2014**, *43*, 5067−5088.

(2) (a) Lambert, C.; Nöll, G. *J. Am. Chem. Soc.* **1999**, *121*, 8434−8442. (b) Hankache, J.; Wenger, O. S. *Chem. Rev.* **2011**, *111*, 5138−5178. (c) Kaupp, M.; Renz, M.; Parthey, M.; Stolte, M.; Würthner, F.; Lambert, C. *Phys. Chem. Chem. Phys.* **2011**, *13*, 16973−16986.

(3) (a) Nelsen, S. F.; Tran, H. Q.; Nagy, M. A. *J. Am. Chem. Soc.* **1998**, *120*, 298−304. (b) Dehareng, D.; Dive, G.; Moradpour, A. *Int. J. Quantum Chem.* **2000**, *76*, 552−573. (c) Fernández, E.; Blancafort, L.; Olivucci, M.; Robb, M. A. *J. Am. Chem. Soc.* **2000**, *122*, 7528−7533. (d) Szeghalmi, A. V.; Edrmann, M.; Engel, V.; Schmitt, M.; Amthor, S.; Kriegisch, V.; Nöll, G.; Stahl, R.; Lambert, C.; Leusser, D.; Stalke, D.; Zabel, M.; Popp, J. *J. Am. Chem. Soc.* **2004**, *126*, 7834−7845. (e) Nelsen, S. F.; Weaver, M. N.; Telo, J. P.; Lucht, B. L.; Barlow, S. *J. Org. Chem.* **2005**, *70*, 9326−9333.

(4) Su, Y.; Wang, X.; Li, Y.; Song, Y.; Sui, Y.; Wang, X. *Angew. Chem., Int. Ed.* **2015**, *54*, 1634−1637.

(5) Kaim, W.; Schulz, A. *Angew. Chem., Int. Ed. Engl.* **1984**, *23*, 615−616.

(6) (a) Low, P. J.; Paterson, M. A. J.; Puschmann, H.; Goeta, A. E.; Howard, J. A. K.; Lambert, C.; Cherryman, J. C.; Tackley, D. R.; Leeming, S.; Brown, B. *Chem. - Eur. J.* **2004**, *10*, 83−91. (b) Littleford, R. E.; Paterson, M. A. J.; Low, P. J.; Tackley, D. R.; Jayes, L.; Dent, G.; Cherryman, J. C.; Brown, B.; Smith, W. E. *Phys. Chem. Chem. Phys.* **2004**, *6*, 3257−3263. (c) Su, Y.; Wang, X.; Zheng, X.; Zhang, Z.; Song, Y.; Sui, Y.; Li, Y.; Wang, X. *Angew. Chem., Int. Ed.* **2014**, *53*, 2857−2861.

(7) (a) Lichtblau, A.; Kaim, W.; Schulz, A.; Stahl, T. *J. Chem. Soc., Perkin Trans. 2* **1992**, 1497−1501. (b) Fiedler, J.; Zali, S.; Klein, A.; Hornung, F. M.; Kaim, W. *Inorg. Chem.* **1996**, *35*, 3039−3043. (c) Kaim, W.; Hosmane, N. S.; Zališ, S.; Maguire, J. A.; Lipscomb, W. *Angew. Chem., Int. Ed.* **2009**, *48*, 5082−5091.

(8) (a) Yamabe, T.; Yamashita, S.; Yamabe, H.; Fukui, K.; Tanaka, K. *Collect. Czech. Chem. Commun.* **1988**, *53*, 1881−1889. (b) Stein, S. E. *Acc. Chem. Res.* **1991**, *24*, 350−356. (c) Yoshizawa, K.; Okahara, K.; Sato, T.; Tanaka, K.; Yamabe, T. *Carbon* **1994**, *32*, 1517−1522. (d) Nakada, K.; Fujita, M.; Dresselhaus, G.; Dresselhaus, M. S. *Phys. Rev. B: Condens. Matter Mater. Phys.* **1996**, *54*, 17954−17961.

(9) (a) Sagara, Y.; Mutai, T.; Yoshikawa, I.; Araki, K. *J. Am. Chem. Soc.* **2007**, *129*, 1520−1521. (b) Sonar, P.; Soh, M. S.; Cheng, Y. H.; Henssler, J. T.; Sellinger, A. *Org. Lett.* **2010**, *12*, 3292−3295. (c) Crawford, A. G.; Dwyer, A. D.; Liu, Z.; Steffen, A.; Beeby, A.; Pålsson, L.-O.; Tozer, D. J.; Marder, T. B. *J. Am. Chem. Soc.* **2011**, *133*, 13349−13362. (d) Lambert, C.; Ehbets, J.; Rausch, D.; Steeger, M. *J. Org. Chem.* **2012**, *77*, 6147−6154. (e) Niko, Y.; Kawauchi, S.; Konishi, G. *Chem. - Eur. J.* **2013**, *19*, 9760−9765. (f) Niko, Y.; Cho, Y.; Kawauchi, S.; Konishi, G. *RSC Adv.* **2014**, *4*, 36480−36484. (g) Matsumoto, A.; Suzuki, M.; Kuzuhara, D.; Yuasa, J.; Kawai, T.; Aratani, N.; Yamada, H. *Chem. Commun.* **2014**, *50*, 10956−10958. (h) Ji, L.; Lorbach, A.; Edkins, R. M.; Marder, T. B. *J. Org. Chem.* **2015**, *80*, 5658−5665.

(10) (a) CCoventry, D. N.; Batsanov, A. S.; Goeta, A. E.; Howard, J. A. K.; Marder, T. B.; Perutz, R. N. *Chem. Commun.* **2005**, 2172−2174. (b) Crawford, A. G.; Liu, Z.; Mkhalid, I. A. I.; Thibault, M.-H.; Schwarz, N.; Alcarez, G.; Steffen, A.; Collings, J. C.; Batsanov, A. S.; Howard, J. A. K.; Marder, T. B. *Chem. - Eur. J.* **2012**, *18*, 5022−5035. (c) Nie, H.-J.; Yao, C.-J.; Shao, J.-Y.; Yao, J.; Zhong, Y.-W. *Chem. - Eur. J.* **2014**, *20*, 17454−17465. (d) Ji, L.; Fucke, K.; Bose, S. K.; Marder, T. B. *J. Org. Chem.* **2015**, *80*, 661−665.

(11) Note that the present compound **3** is very similar to one reported by Marder and co-workers (see compound **16** in ref 10b).

(12) (a) Yao, C.-J.; Sui, L.-Z.; Xie, H.-Y.; Xiao, W.-J.; Zhong, Y.-W.; Yao, J. *Inorg. Chem.* **2010**, *49*, 8347−8350. (b) Yao, C.-J.; Nie, H.-J.; Yang, W.-W.; Yao, J.; Zhong, Y.-W. *Inorg. Chem.* **2015**, *54*, 4688−4698.

(13) (a) Yao, C.-J.; Yao, J.; Zhong, Y.-W. *Inorg. Chem.* **2011**, *50*, 6847−6849. (b) Nie, H.-J.; Chen, X.; Yao, C.-J.; Zhong, Y.-W.; Hutchison, G. R.; Yao, J. *Chem. - Eur. J.* **2012**, *18*, 14497−14509.

(14) Nie, H.-J.; Yao, C.-J.; Shao, J.-Y.; Yao, J.; Zhong, Y.-W. *Chem. - Eur. J.* **2014**, *20*, 17454−17465.

(15) Ji, L.; Edkins, R. M.; Lorbach, A.; Kummenacher, I.; Brückner, C.; Eichhorn, A.; Braunschweig, H.; Engels, B.; Low, P. J.; Marder, T. B. *J. Am. Chem. Soc.* **2015**, *137*, 6750−6753.

(16) (a) Barlow, S.; Risko, C.; Coropceanu, V.; Tucker, N. M.; Jones, S. C.; Levi, Z.; Khrustalev, V. N.; Antipin, M. Y.; Kinnibrugh, T. L.; Timofeeva, T.; Marder, S. R.; Bredas, J.-L. *Chem. Commun.* **2005**, 764−766. (b) Zheng, S.; Barlow, S.; Risko, C.; Kinnibrugh, T. L.; Khrustalev, V. N.; Jones, S. C.; Antipin, M. Y.; Tucker, N. M.; Tomofeeva, T. V.; Coropceanu, V.; Bredas, J.-L.; Marder, S. R. *J. Am. Chem. Soc.* **2006**, *128*, 1812−1817.

(17) Synthetic procedures for compound **3** are described in the Supporting Information. The compound **3** exhibited photoluminescence with emission maximum at λ = 520 nm in 0.01 mM CH_2Cl_2 solution with Φ = 0.094 at room temperature under irradiation with light (λ_{ex} = 330 nm).

(18) (a) Hartwig, J. F. *Acc. Chem. Res.* **2008**, *41*, 1534−1544. (b) Muci, A. R.; Buchwald, S. L. *Top. Curr. Chem.* **2002**, *219*, 131−209.

(19) Dietrich, M.; Heinze, J. *J. Am. Chem. Soc.* **1990**, *112*, 5142−5145.

(20) Meerholz, K.; Heinze, J. *Electrochim. Acta* **1996**, *41*, 1839−1854.

(21) Adams, B. K.; Cherry, W. R. *J. Am. Chem. Soc.* **1981**, *103*, 6904−6907.

(22) Nelsen, S. F. *Chem. - Eur. J.* **2000**, *6*, 581−588.

(23) (a) Bell, F. A.; Ledwith, A.; Sherrington, D. C. *J. Chem. Soc. C* **1969**, 2719. (b) Connelly, N. G.; Geiger, W. E. *Chem. Rev.* **1996**, *96*, 877−910.

(24) In the calculations of vertical excitation energies on polycyclic aromatic hydrocarbons including pyrene, the use of CAM-B3LYP functional have recently been known to be better than the use of the B3LYP functional, as has been pointed out in ref 9c. However, in the present compound **3**, the B3LYP functional gave better results: for instance, the lowest energy band at around 2.5 eV and the next lowest energy band at around 3.8 eV observed for neutral **3** were calculated to be 2.58 and 3.72 eV with B3LYP, respectively (Figure S3 in the SI), whereas the CAM-B3LYP functional gave 3.27 and 4.24 eV, respectively. Hence, throughout the present work, we employed the B3LYP functional.

(25) Kuprat, M.; Lehmann, N.; Schulz, A.; Villinger, A. *Organometallics* **2010**, *29*, 1421−1427.

(26) Krossing, I.; Raabe, I. *Angew. Chem., Int. Ed.* **2004**, *43*, 2066−2090.

(27) Selected X-ray data for **3**, $\mathbf{3}^{\bullet+}\cdot[B(C_6F_5)_4]^-$, and $\mathbf{3}^{2+}\cdot 2[B(C_6F_5)_4]^-$ are listed in Table S1 (Supporting Information). CCDC 1404354 (**3**), 1404355 ($\mathbf{3}^{\bullet+}$), and 1404356 ($\mathbf{3}^{2+}$) contain the

DOI: 10.1021/acs.joc.5b02425
J. Org. Chem. 2016, 81, 137−145

supplementary crystallographic data. These data can be obtained free of charge from the Cambridge Crystallogarphic Data Centre via www.ccdc.cam.ac.uk/data_request/cif.
(28) The NICS values over the pyrene moiety also gradually changed on going from **3** to $\mathbf{3}^{2+}$; see Figure S10 in the Supporting Information.
(29) Ravat, P.; Teki, Y.; Ito, Y.; Gorelik, E.; Baumgarten, M. *Chem. - Eur. J.* **2014**, *20*, 12041−12045.
(30) Bleaney, B.; Bowers, K. D. *Proc. R. Soc. London, Ser. A* **1952**, *214*, 451−465.
(31) Trinquier, G.; Suaud, N.; Malrieu, J.-P. *Chem. - Eur. J.* **2010**, *16*, 8762−8772.
(32) Gupta, R. R. *Landolt-Börnstein, New Series II*; Hellwege, K.-H., Hellwege, A. M., Eds.; Springer Verlag: Berlin, 1986; Vol. *16* (Diamagnetic Susceptibility).
(33) Ragavachari, K. *Theor. Chem. Acc.* **2000**, *103*, 361−363 and references cited therein.
(34) Dreuw, A.; Head-Gordon, M. *Chem. Rev.* **2005**, *105*, 4009−4037.
(35) Hehre, W. J.; Radom, L.; Schleyer, P. v. R.; Pople, J. A. *Ab Initio Molecular Orbital Theory*; Wiley: New York, 1986.
(36) Frisch, M. J.; Trucks, G. W.; Schlegel, H. B.; Scuseria, G. E.; Robb, M. A.; Cheeseman, J. R.; Scalmani, G.; Barone, V.; Mennucci, B.; Petersson, G. A.; Nakatsuji, H.; Caricato, M.; Li, X.; Hratchian, H. P.; Izmaylov, A. F.; J. Bloino, J.; Zheng, G.; Sonnenberg, J. L.; Hada, M.; Ehara, M.; Toyota, K.; Fukuda, R.; Hasegawa, J.; Ishida, M.; Nakajima, T.; Honda, Y.; Kitao, O.; Nakai, H.; Vreven, T.; Montgomery, Jr., J. A.; Peralta, J. E.; Ogliaro, F.; Bearpark, M.; Heyd, J. J.; Brothers, E.; Kudin, K. N.; Staroverov, V. N.; Keith, T.; Kobayashi, R.; Normand, J.; Raghavachari, K.; Rendell, A.; Burant, J. C.; Iyengar, S. S.; Tomasi, J.; Cossi, M.; Rega, N.; Millam, J. M.; Klene, M.; Knox, J. E.; Cross, J. B.; Bakken, V.; Adamo, C.; Jaramillo, J.; Gomperts, R.; Stratmann, R. E.; Yazyev, O.; Austin, A. J.; Cammi, R.; Pomelli, C.; Ochterski, J. W.; Martin, R. L.; Morokuma, K.; Zakrzewski, V. G.; Voth, G. A.; Salvador, P.; Dannenberg, J. J.; Dapprich, S.; Daniels, A. D.; Farkas, O.; Foresman, J. B.; Ortiz, J. V.; Cioslowski, J.; Fox, D. J. *Gaussian 09*, Revision D.01; Gaussian, Inc.: Wallingford, CT, 2013.
(37) *CrystalStructure 4.1, Crystal Structure Analysis Package*; Rigaku Corporation: Tokyo, Japan, 2000−2014; pp 196−8666.
(38) Sheldrick, G. M. *Acta Crystallogr., Sect. A: Found. Crystallogr.* **2008**, *64*, 112−122.

DOI: 10.1021/acs.joc.5b02425
J. Org. Chem. 2016, 81, 137−145